

Digital Beamforming Demonstration of a Microstrip Antenna Phased Array Feeds (PAF) at 1.25 GHz

Peng Wu (作鵬)^{1,2,3,4}, Mao-Zheng Chen (陈卯蒸)^{1,3,4}, Jian Li (李健)^{1,2,3,4}, Kai Wang (王凯)^{1,3}, Liang Cao (曹亮)^{1,3}, and Han Yu (于涵)^{1,3}

¹ Xinjiang Astronomical Observatory, Chinese Academy of Sciences, Urumqi 830011, China; wupeng@xao.ac.cn, chen@xao.ac.cn, lijian@xao.ac.cn

² University of Chinese Academy of Sciences, Beijing 100049, China

³ Xinjiang Key Laboratory of Microwave Technology, Urumqi 830011, China

*Received 2024 June 13; revised 2024 August 4; accepted 2024 August 29; published 2024 September 25

Abstract

We introduce the structure of a radio astronomy phased array feeds (PAF) beamforming demonstrator. In a laboratory environment, we have demonstrated beamforming on a received 1.25 GHz sinusoidal signal and used digital weighting techniques to plot the 2D pattern of the PAF. The radio frequency part of the demonstrator includes a 4×4 linearly polarized microstrip antenna array, all of which is connected in series with a low-noise amplifier. The signals from the central 4×2 array elements are injected into a radio frequency system-on-chip digital board, which can receive eight inputs with a bandwidth of 512 MHz. Combining the principle of undersampling, the beamforming is completed at a frequency of 1.25 GHz for the offline data, and a 2D image of the beam is plotted using beam scanning technology.

Key words: Astronomical Instrumentation – Methods and Techniques – Astronomical Databases – methods: data analysis

1. Introduction

Faster sky survey speed is an important means for new discoveries in radio astronomy. Phased array feeds (PAF) receivers located at the focal plane of the telescope can achieve continuous sky coverage, thereby improving the measurement speed (Warnick et al. 2016; Roshi et al. 2018). A PAF performs spatial sampling on the focal plane to generate time-domain array voltage signals. Through digital control of the complex weights (phase and amplitude) of each element, multiple independent beams can be generated and form a continuous field-of-view (FoV). At the same time, each beam can be independently optimized, resulting in higher aperture efficiency and lower sidelobe spillover (Navarrini et al. 2022). So, a PAF combines the advantages of traditional reflector antennas' high gain, low sidelobe level, and low cost per unit aperture area with the multibeam capabilities and wider FoV of phased arrays (Warnick et al. 2016).

We have established a 4×4 array of microstrip antennas with vertical polarization, as shown in Figure 1(1). The central 4×2 array elements are used to form a beam, and the number of these elements matches the number of analog-to-digital converters (ADCs) on the commercial Zynq UltraScale+ radio frequency system-on-chip (RFSoC) ZCU111 board. We use a ridged waveguide horn antenna to transmit a 1.25 GHz

sinusoidal signal as demonstrated in Figure 1(2) and (3). The analog signals generated by the PAF in far field are amplified by a low-noise amplifier (LNA) and then input into the Zynq UltraScale+ RFSoC ZCU111 board, with the ADC's sampling bandwidth set to 512 MHz. According to the aliasing principle, the spectrum of the transmitted signal will be observed at 226 MHz. We rely on a digital filter to extract the signal and then calibrate the phase of the signal. Finally, we implement digital beamforming to scan the PAF within a range of 180° in the horizontal and vertical directions. This is the first time that such kind of beamforming has been achieved in a laboratory.

2. Experimental Platform

Figures 1 and 2 illustrate the complete architecture of signal transmission and reception. The transmission part is generated by a signal generator that produces a 1.25 GHz sine wave signal, which is radiated into space by a ridged waveguide horn antenna. The maximum diameter D of the horn antenna is approximately 0.3 m. According to the far-field formula $R=2D^2/\lambda$, where λ is the wavelength of the 1.25 GHz signal, the far-field distance should be greater than 0.75 m. The actual placement distance of the microstrip array antenna is about 4.13 m, which meets the far-field conditions. The 4×2 array elements used for receiving adopt the same signal chain, and each element is cascaded with an amplifier. The microstrip antenna features a design with an embedded feed and radiating edge (radiating edge with inset feed), with a measured center

⁴ Authors to whom any correspondence should be addressed.

⁵ https://china.xilinx.com/products/boards-and-kits/zcu111.html

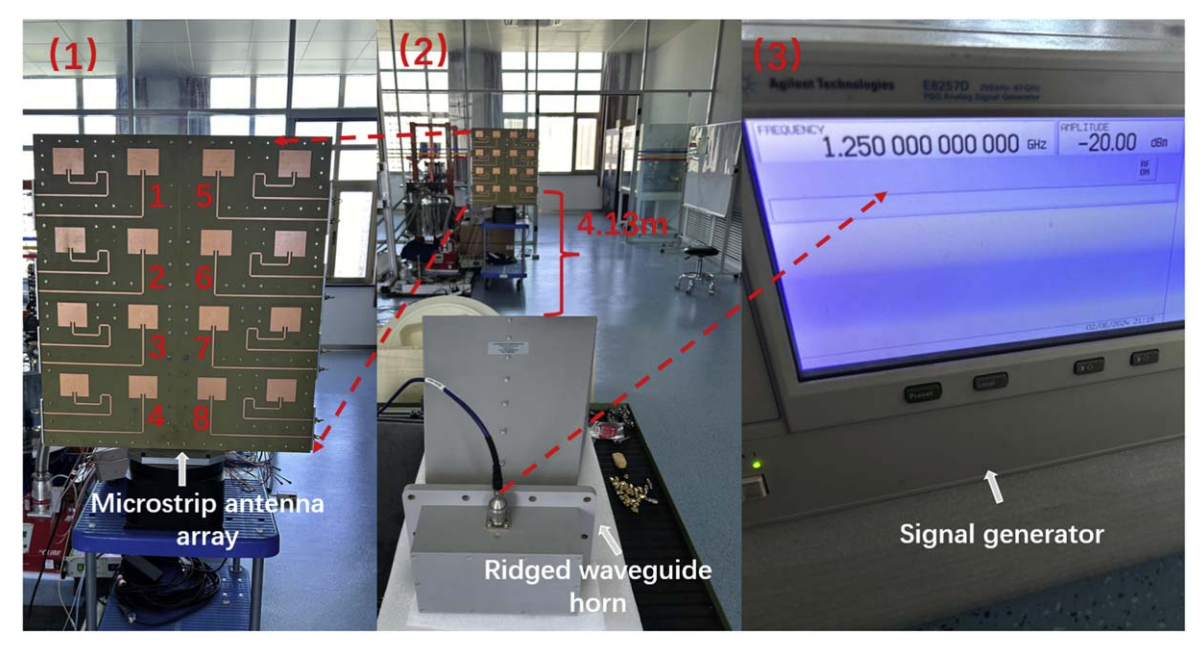


Figure 1. (1) A 4×4 microstrip antenna array with element 3 serving as the reference element. (2) Ridge waveguide horn antenna radiating a signal to the PAF. (3) The signal generator produces a 1.25 GHz sine wave signal with a strength of -20 dB.

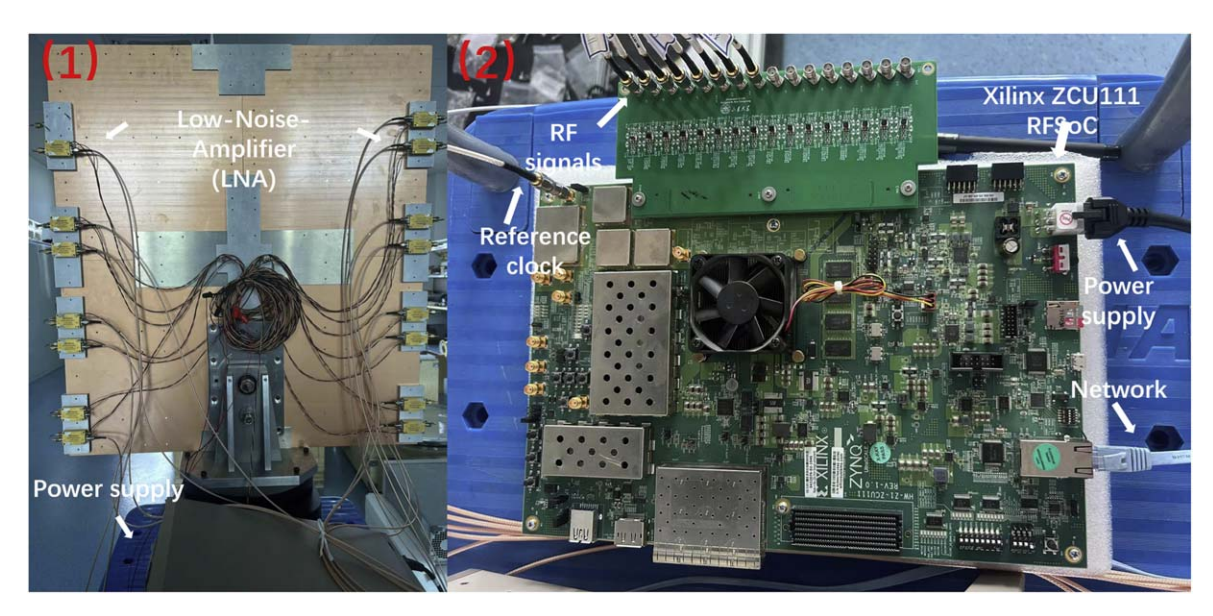


Figure 2. (1) The cascade between array antenna and LNA. (2) Eight channels of radio frequency (RF) signals are connected to the digital RFSoC board, and the sandwich board shown above will be used to connect the Zynq UltraScale+ RFSoC ZCU111 to the RF module.

frequency of 1.27 GHz and an effective bandwidth of 1.24–1.29 GHz. The amplifier is calibrated to operate over a bandwidth of 0.01–3 GHz with a gain of 30 dB. The output signal of the amplifier is injected into a Zynq UltraScale+RFSoC ZCU111 board for analog-to-digital conversion. This board communicates with a PC and downloads data through a network switch. The development of the digital portion utilizes

the CASPER Toolflow,⁶ with the ADC's sampling frequency set to $1024\,\mathrm{MHz}$ and a quantization precision of 8 bits. According to the principle of spectrum aliasing and bandwidth of the PAF, a frequency of $1.25\,\mathrm{GHz}$ can be observed at $1.25\,\mathrm{GHz}$ % $512\,\mathrm{MHz} = 226\,\mathrm{MHz}$, where "%" represents the

⁶ https://casper-toolflow.readthedocs.io/en/latest/

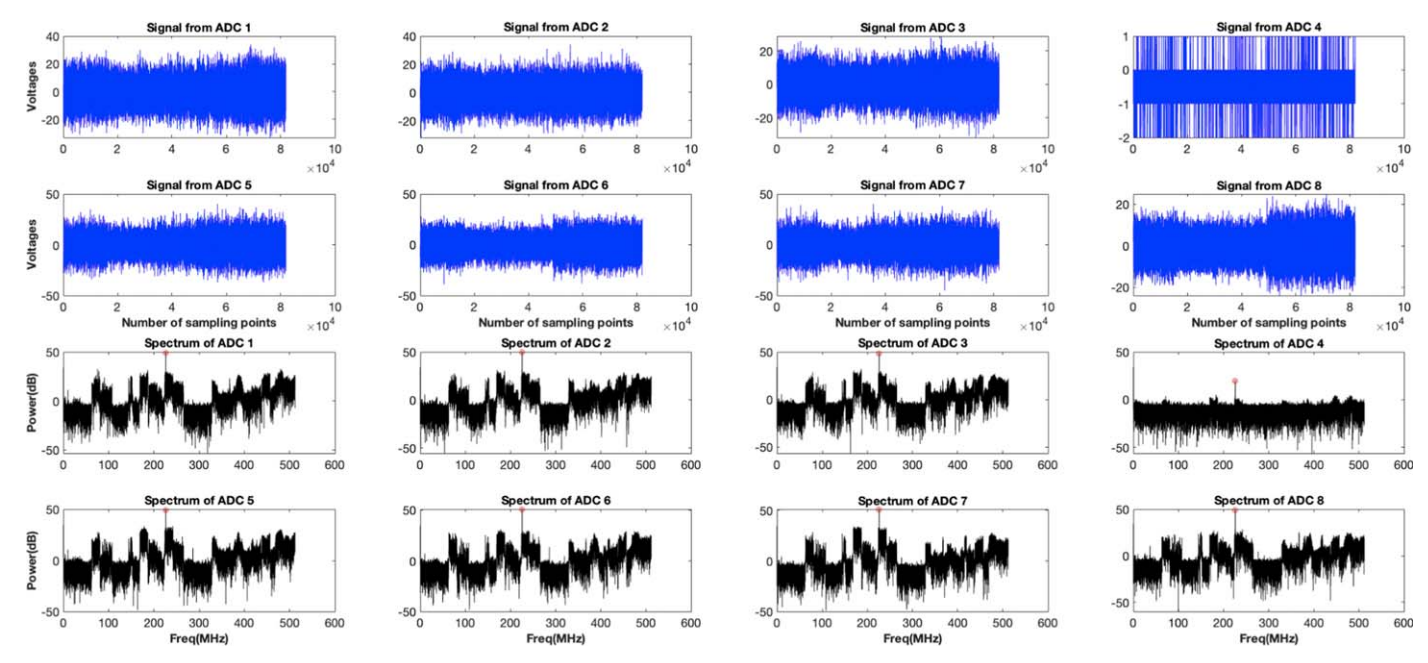


Figure 3. Received signal image when the signal generator is turned on, the blue line image is the voltage image of eight RF signals, and the black line image is the corresponding spectrum image.

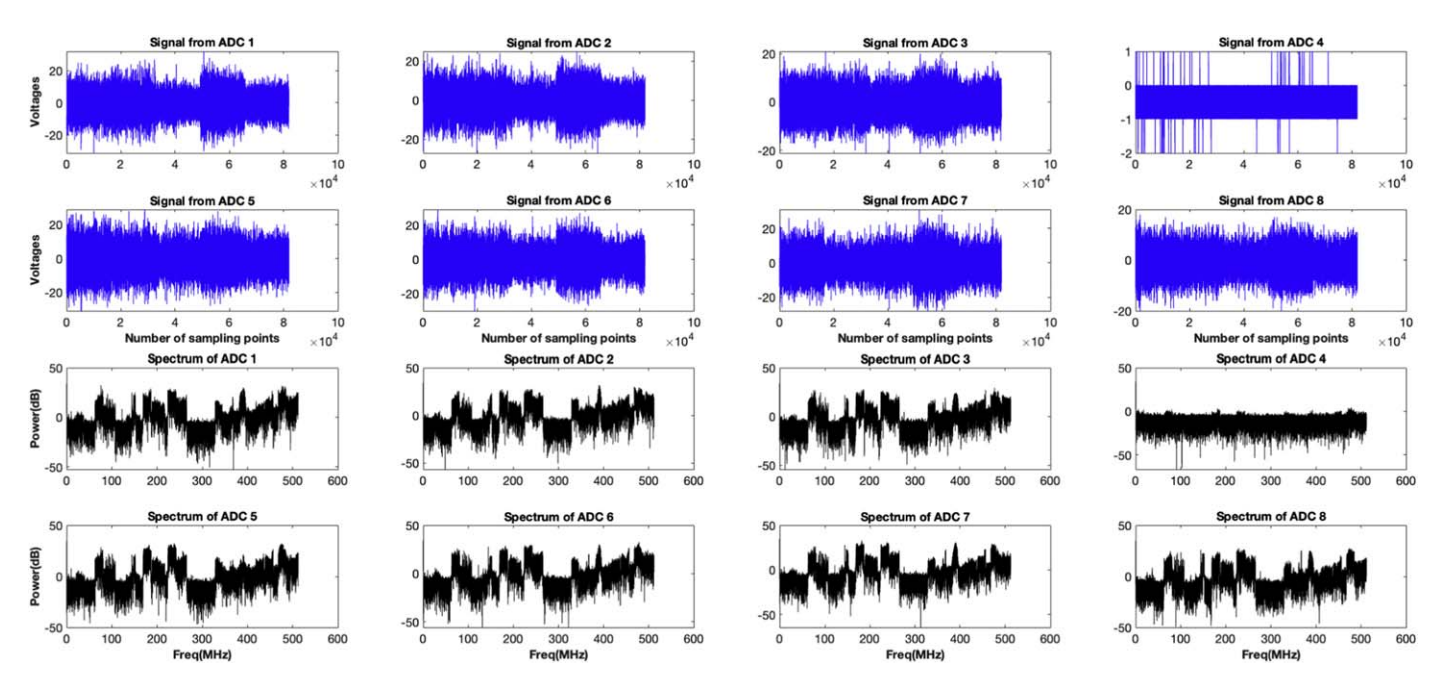


Figure 4. Received signal image when the signal generator is turned off, the blue line image is the voltage image of eight RF signals, and the black line image is the corresponding spectrum image.

modulo operation. The size of a data packet is limited to 16,384 (16 μ s), and five packets are captured at a time. It is important to note that these five data packets are not strictly continuous in

time. However, since the experimental environment is fixed, they can be treated as a continuous time series for processing together.

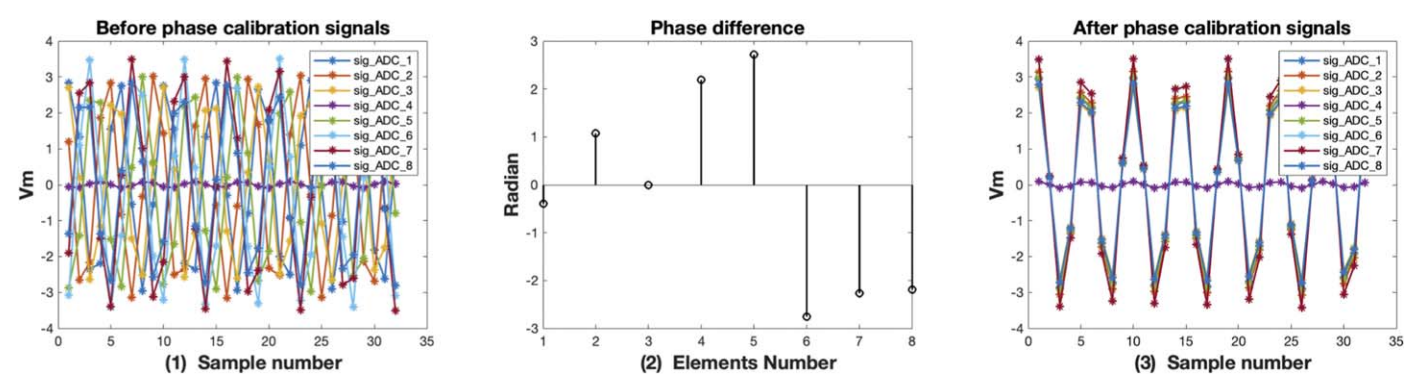


Figure 5. (1) Time domain signal before phase calibration. (2) Phase difference between each element and the reference element. (3) Time domain signal after phase calibration.

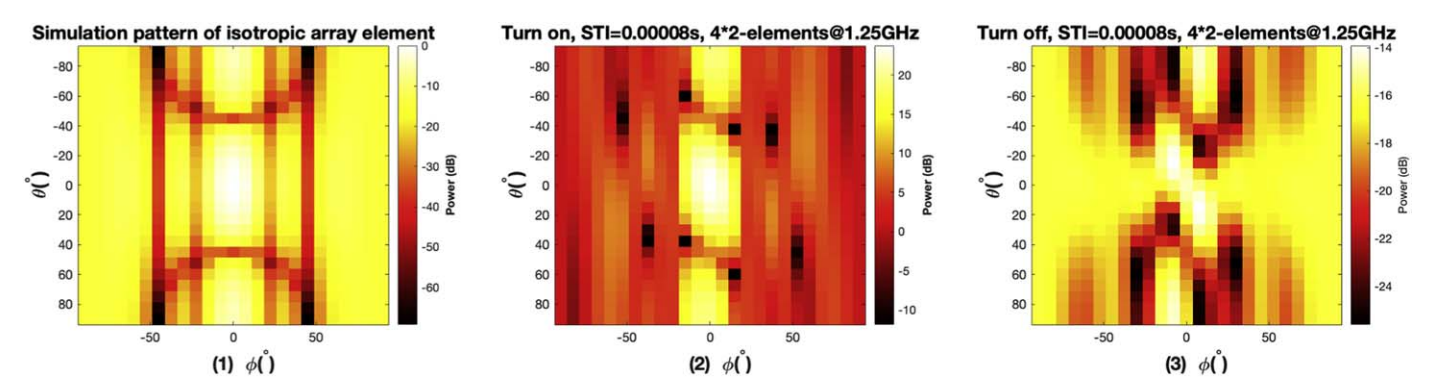


Figure 6. (1) Simulated pattern of isotropic array element beamforming. (2) Beamforming image when the signal generator is turned on. (3) Beamforming image when the signal generator is turned off.

3. Digital Signal Processing and Beamforming

As displayed in Figures 3 and 4, the temporal distribution and spectrum of the captured data are described. Figure 3 illustrates the data distribution when the signal generator is turned on, while Figure 4 describes the data distribution when the signal generator is turned off. The red marked part of the spectrum diagram in Figure 3 is the received signal spectrum. It is noted that during testing, due to the failure of LNA of the fourth array element, the signal from that channel was not amplified. Therefore, the signal reference value of this channel is negligible during the subsequent beamforming process.

We employ a notch filter to eliminate all signals outside the 226 MHz range. Prior to beamforming, it is necessary to calibrate the phase of the received signal in order to compensate for errors such as those arising from the LNA, signal lines, interface, PAF misalignment due to gravity-induced non-coplanarity, and horizontal illumination level of the ridge waveguide horn. The greatest impact on the phase of the received signal stems from LNA, which is attributed to inconsistencies in its phase-frequency characteristics. With element 3 as the reference, Figure 5(1) depicts the time domain signal of each element after filtering and computes the phase

difference relative to the reference. The results are presented in Figure 5(2). We conducted frequency domain phase compensation for each array element, and the time-domain representation of the compensated signals is depicted in Figure 5(3).

Placing the PAF in the yoz plane of the Cartesian coordinate system, the phase difference between the mth element and the reference element can be described as: $\Delta \phi_m = \Delta \phi_m^y +$ $\Delta \phi_m^z = \frac{2\pi}{\lambda} (d_m^y \cos \theta \sin \phi + d_m^z \sin \theta)$, where $\Delta \phi_m^y$ and $\Delta \phi_m^z$ represent the spatial phase differences along the y-axis and zaxis, respectively, d_m^y and d_m^z are the distances from the reference element along the y-axis and z-axis, respectively, θ is the elevation angle and ϕ is the azimuth angle (Li et al. 2023). Therefore, the unit beam steering vector can be expressed as $w(\theta, \phi) = [e^{j\Delta\phi_1(\theta,\phi)}, e^{j\Delta\phi_2(\theta,\phi)}, ..., e^{j\Delta\phi_m(\theta,\phi)}],$ and the received power in the direction (θ_0, ϕ_0) can be expressed as $P(\theta_0, \phi_0) = w(\theta_0, \phi_0)^H R_x w(\theta_0, \phi_0)$, where R_x is the correlation matrix of the received signal and $(\cdot)^{H}$ denotes the conjugate transpose operation. We conducted a digital scan of the data from Figures 3 and 4 in the range of θ : 0°-180° and ϕ : -90°-90°, and the scanning results are shown below with a resolution of 25×25 (Wu et al. 2024). Figure 6 presents the twodimensional (2D) image resulting from beamforming.

Figure 6(1) illustrates the simulated pattern (normalized) for an isotropic antenna used as the array element. Figure 6(2) depicts the response image captured when the signal generator is activated, while Figure 6(3) also represents the response image obtained with the signal generator deactivated. It is important to note that the signal processing techniques applied in Figure 6(2) and (3) are identical, encompassing phase compensation. The image outcomes clearly demonstrate that when the horn antenna emits the signal, brighter images and elevated power levels are achievable.

4. Conclusion

This paper introduces the demonstration device of microstrip PAF digital beamforming, and describes the process of transmitting, collecting and processing the experimental signal in detail. This is the first time that we use digital weighting to realize the beamforming of a 2D power image of PAF, which lays a good foundation for our subsequent wideband multiple beamforming.

Acknowledgments

This work is funded by the National Key R&D Program of China under No. 2022YFC2205300, the National Natural Science Foundation of China (NSFC, grant Nos. 12073067 and 11973078), and the Chinese Academy of Sciences (CAS) "Light of West China" Program under No. 2022-XBQNXZ-012 and No. 2020-XBQNXZ-018. Thanks go to Dr. Duan Ran of the National Astronomical Observatories for providing the Zynq UltraScale+ RFSoC ZCU111 board.

References

Li, J., Wu, P., Duan, X., et al. 2023, AcASn, 64, 2

Navarrini, A., Melis, A., Comoretto, G., et al. 2022, in 2022 3rd URSI Atlantic and Asia Pacific Radio Science Meeting (AT-AP-RASC) (Gran Canaria: 3 rd URSI AT-AP-RASC), 1

Roshi, D. A., Shillue, W., Simon, B., et al. 2018, AJ, 155, 202

Warnick, K. F., Maaskant, R., Ivashina, M. V., Davidson, D. B., & Jeffs, B. D. 2016, Proc. IEEE, 104, 607

Wu, P., Li, J., & Chen, M.-Z. 2024, RAA, 24, 015019